

Relationship between the Arctic oscillation and surface air temperature in multi-decadal time-scale

著者	Tanaka Hiroshi L., Tamura Mina
journal or publication title	Polar science
volume	10
number	3
page range	199-209
year	2016-09
権利	(C) 2016 The Authors. Published by Elsevier B.V. This is an open access article under the CC BY-NC-ND license (http://creativecommons.org/licenses/by-nc-nd/4.0/).
URL	http://hdl.handle.net/2241/00144341

doi: 10.1016/j.polar.2016.03.002



Relationship between the Arctic oscillation and surface air temperature in multi-decadal time-scale



Hiroshi L. Tanaka ^{a, *}, Mina Tamura ^b

^a Center for Computational Sciences, Univ. of Tsukuba, Japan

^b Graduate School of Life and Environmental Sciences, Univ. of Tsukuba, Japan

ARTICLE INFO

Article history:

Received 2 November 2015

Received in revised form

14 February 2016

Accepted 6 March 2016

Available online 16 March 2016

Keywords:

Arctic oscillation

Arctic amplification

Energy balance model

Planetary albedo

Multi-decadal variability

ABSTRACT

In this study, a simple energy balance model (EBM) was integrated in time, considering a hypothetical long-term variability in ice-albedo feedback mimicking the observed multi-decadal temperature variability. A natural variability was superimposed on a linear warming trend due to the increasing radiative forcing of CO₂. The result demonstrates that the superposition of the natural variability and the background linear trend can offset with each other to show the warming hiatus for some period. It is also stressed that the rapid warming during 1970–2000 can be explained by the superposition of the natural variability and the background linear trend at least within the simple model.

The key process of the fluctuating planetary albedo in multi-decadal time scale is investigated using the JRA-55 reanalysis data. It is found that the planetary albedo increased for 1958–1970, decreased for 1970–2000, and increased for 2000–2012, as expected by the simple EBM experiments. The multi-decadal variability in the planetary albedo is compared with the time series of the AO mode and Barents Sea mode of surface air temperature. It is shown that the recent AO negative pattern showing warm Arctic and cold mid-latitudes is in good agreement with planetary albedo change indicating negative anomaly in high latitudes and positive anomaly in mid-latitudes. Moreover, the Barents Sea mode with the warm Barents Sea and cold mid-latitudes shows long-term variability similar to planetary albedo change. Although further studies are needed, the natural variabilities of both the AO mode and Barents Sea mode indicate some possible link to the planetary albedo as suggested by the simple EBM to cause the warming hiatus in recent years.

© 2016 The Authors. Published by Elsevier B.V. This is an open access article under the CC BY-NC-ND license (<http://creativecommons.org/licenses/by-nc-nd/4.0/>).

1. Introduction

Recent global warming is characterized by an Arctic amplification as was predicted by pioneer studies by Manabe and Wetherald (1975) and Manabe and Stouffer (1980). The Arctic amplification is a response to the anthropogenic radiative forcing by increasing greenhouse gases such as CO₂. When the radiative forcing acts as uniform warming of the atmosphere, the Arctic warms more than the global average. For example, when the global mean temperature warms 2.0 °C, the Arctic tends to warm 5.0 °C, which is 2.5 times larger than the global mean. Likewise, when the radiative forcing acts uniform cooling of the atmosphere, the Arctic cools more than the global average. The arctic amplification is an

enhanced response of the Arctic to both warming and cooling. When the response is argued not only for the Arctic but also for the Antarctic, the naming of polar amplification is used for a general case (Langen and Alexeev, 2007).

The mechanism of the Arctic amplification was explained mostly by the ice-albedo feedback occurring in the cryosphere in high latitudes. The short wave radiation is reflected back to the space by the surface high albedo over the cryosphere, which cools the climate system more to expand the cryosphere in high latitudes. This strong feedback operates at the subarctic where the sun shine can reach in winter season. According to the comprehensive diagnostic analysis of the climate system models (Yoshimori et al., 2009, 2014), the Arctic amplification is induced not only by the ice-albedo feedback but also by many other processes, including the enhanced meridional heat transport by the atmosphere and ocean, changes of long-wave radiation by cloud amount or moisture in the atmosphere, changes of lapse rate and vertical temperature profile with strong inversion, and

* Corresponding author. Center for Computational Sciences, University of Tsukuba, 1-1-1 Tennoudai, Tsukuba, Ibaraki 305-8577, Japan.

E-mail address: tanaka@ccs.tsukuba.ac.jp (H.L. Tanaka).

radiation changes by black carbon aerosol or life activity in snow at microscopic scales. Those processes are mutually related in a complex way to cause the robust Arctic amplification. However, we aware that the ice-albedo feedback is the most important process among those according to the quantitative comparison of each process by the variational method in response to the prescribed radiative forcing due to the increasing greenhouse gases (Yoshimori et al., 2009, 2014).

The anthropogenic Arctic warming is superimposed by natural (or internal) variability, such as the Arctic oscillation (AO) in the atmosphere, or Pacific decadal-oscillation (PDO) and Atlantic multi-decadal oscillation (AMO) in the ocean (Trenberth and Fasullo, 2013; Wallace and Thompson, 2002). The AO is defined by the first empirical orthogonal function (EOF) of the sea level pressure (SLP) having low pressure anomaly in the Arctic and high pressure anomaly in mid-latitudes with the node at 60° N for the positive AO index (Thompson and Wallace, 1998). The polar jet stream is enhanced by the large meridional pressure gradient. The corresponding regression map for surface air temperature (SAT) shows cold anomaly in the Arctic and Greenland and warm anomaly in mid-latitudes especially over northern Siberia for the positive AO index. Those patterns in pressure, wind, and temperature reverse for the negative AO index.

According to the EOF analysis of the monthly mean SAT during winter by Nagato and Tanaka (2012), the AO mode appears as the EOF-1 with 24% of variance, and the Arctic amplification mode appears as the EOF-2 with 15% of variance. The EOF-3 is characterized by warm anomaly over Barents Sea and cold anomaly in mid-latitude, especially over southern Siberia counting 12% of variance. The time series of the EOF-1 for AO is called AO index, showing decreasing trend for 1950–1970, increasing trend for 1970–1990, and decreasing trend for 1990–2010, indicating multi-decadal variability. Since the observed warming pattern in temperature coincides with that of AO for 1970–1990, explaining 40% of variance, AO was considered as one of the causes of the global warming (Shindell et al., 1999). Yet, the AO index started to decrease after 1990 while the mean temperature keeps increasing. The AO thus turns to be excluded from the possible candidate for the cause of global warming.

After the year 1998 of strong El-Niño, global mean temperature halted the increase, despite the monotonic increase of CO₂ concentration (Trenberth and Fasullo, 2013). The discrepancy between the monotonic warming prediction by climate models and the actual observation of halting warming is called as a warming hiatus problem. Since the AO index indicates a decreasing trend during the warming hiatus period, and the temperature anomaly turns to show warm Arctic and cold mid-latitude pattern similar to the AO negative pattern, AO turns to draw more attention again in connection to the global warming hiatus (Overland et al., 2011; Mori et al., 2014). Since the AO is a chaotic internal variability in the atmosphere (Hirata et al., 2011), multi-decadal variability of the AO needs to be investigated in more detail.

The global warming hiatus was partly explained by Kosaka and Xie (2013) and Watanabe et al. (2014) by means of the internal variability associated with the PDO. The SST anomaly is similar to La-Niña a pattern indicating cold SST anomaly in the tropical eastern Pacific and warm SST anomaly in the northern Pacific. The mean atmospheric temperature associated with the internal variability indicates a warm phase for 1970–2000 and a cold phase for 2000–2012, which is superimposed on the anthropogenic global warming trend. The warming hiatus was explained by the accumulated heat energy in deep ocean by these studies. However, the mechanism of the energy accumulation in ocean deeper than 2000 m without the temperature increase at the ocean surface needs to be clarified.

In this study we attempt to simulate the multi-decadal variability of the mean temperature using a simple energy balance model (EBM) by Alexeev and Jackson (2012). Here the model is constructed by two control volumes of low-latitudes and high-latitudes separated by 30° N. The balance equations for the heat contents are integrated over the entire control volume. Then the total heat content for each box is governed by the cross-boundary flux and the source sink within each the box. Although the EBM is quite simple, it is based on the rigorous physical laws of conservations. It was demonstrated by previous studies that the model is suitable to explain the mechanism of the Arctic amplification induced by the ice-albedo feedback. We attempt in this study to apply this EBM by including the fluctuation of the boundary flux associated with the ice-albedo feedback. Moreover, the relationship between the multi-decadal variability of mean temperature and planetary albedo is investigated using the long-term reanalysis data in reference to the internal variabilities of the atmosphere.

2. Energy balance model

The energy balance model (EBM) used in this study is based on Alexeev and Jackson (2012), where the climate system in the Northern Hemisphere is divided in low-latitude box 1 and high-latitude box 2 separated by the latitude 30° N as seen in Fig. 1. The thermodynamic energy equation is integrated over the control volume of the entire atmosphere and mixed layer of ocean and land surface within the box. The heat capacity of the system is represented by a constant parameter H . Then the balance equation for total heat energy in the control volume is governed by cross boundary fluxes of short wave S and long wave OLR and a meridional heat transport F . The source and sink term within the box ϵ represents the radiative forcing by doubling CO₂ as a deviation from the present climate. The unique setting of this EBM is a consideration of ice-albedo feedback by the variable ice fraction a over the hemisphere with a constant albedo α in high-latitudes. Refer to Alexeev and Jackson (2012) and Umino (2014) for the detail of the formulation and parameters. Although the governing equations are quite simple, the equation is based on a rigorous fluid mechanics of a balance equation for heat energy of the climate system over the

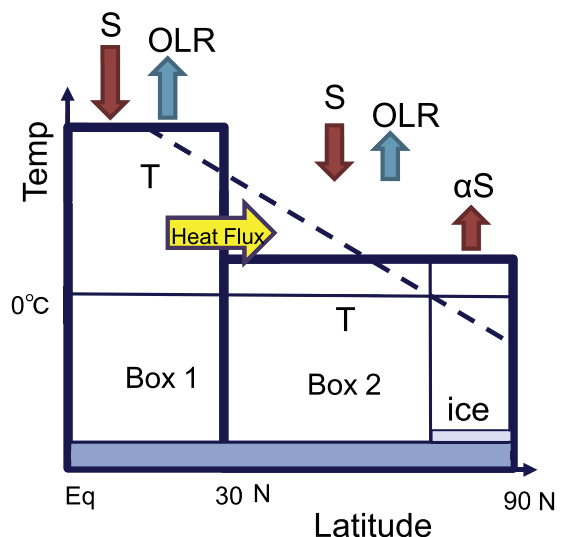


Fig. 1. Schematic picture of the energy balance model (EBM) for Box 1 and Box 2 separated by 30° N. The symbols S and OLR denote short and long wave radiations. A cryosphere (ice) is considered at temperature less than 0° C with higher albedo α .

control volumes as below:

$$H \frac{dT_1}{dt} = S_1 - (C + BT_1) - F + \varepsilon \quad (1)$$

$$H \frac{dT_2}{dt} = S_2(1 - 2\alpha a) - (C + BT_2) + F + \varepsilon \quad (2)$$

here, the long wave radiation has been linearized with constants C and B . The meridional heat transport F is parameterized by a combination of sensible heat flux and latent heat flux as functions of T_1 and T_2 as follows:

$$F = F_0 + \gamma_1(T_1 - T_2) + \gamma_2 C(T_1)(T_1 - T_2), \quad (3)$$

where, F_0 , γ_1 and γ_2 are constants, and $C(T_1)$ is the Tetens approximation to the Clausius–Clapeyron equation as a function of T_1 (see [Alexeev and Jackson, 2012](#) for the detail). It has a characteristic of decreasing sensible heat flux and increasing latent heat flux when global warming takes place showing the Arctic amplification. These two processes offset with each other to show little change of the total heat flux by the global warming as demonstrated by climate model experiments (e.g., [Graversen and Wang, 2009](#); [Kay et al. 2012](#)).

3. Basic analysis of EBM

[Table 1](#) demonstrates the basic properties of the present EBM for the equilibrium of the climate system. In Experiment 1 (E1), no heat flux ($F = 0$) with no cryosphere ($a = 0$) is assumed in the EBM for the present amount of CO_2 ($\varepsilon = 0$). The local temperatures T_1 and T_2 are determined by the local radiative balance, giving the (global) mean temperature $T_G = (T_1 + T_2)/2 = 287$ K with the north–south difference $T_1 - T_2 = 60$ K. Such a large meridional temperature difference is dynamically unstable by the baroclinic instability. Therefore, the meridional heat flux is induced by baroclinic waves, reducing the temperature difference from 60 K to 20 K when the heat flux F is turned on as in Experiment 2 (E2). The heat flux is equilibrated at $F = 5.5$ PW. Here, P (peta) stands for 10^{15} . In Experiment 3 (E3), the cryosphere a is turned on to introduce the ice–albedo feedback. The ice fraction is equilibrated at $a = 0.12$, which corresponds to the ice–edge latitude of 61° N in zonally symmetric ice cap over the Arctic. The mean temperature decreases by 3 K and north–south difference increases by 4 K. We consider that the result for E3 represents the present climate state in the EBM. Finally, in Experiment 4 (E4), the anthropogenic radiative forcing by doubling CO_2 is imposed as a source sink term ε adding 0.51 PW, which corresponds to 4.0 W m^{-2} for each control volume. Mean temperature increases by 3 K as the global warming of T_G in E4–E3, showing Arctic amplification with larger warming in higher latitudes ($\Delta T_2 = 4$) compared to lower latitudes ($\Delta T_1 = 2$) as seen in E4–E3. If we define the Arctic amplification by $A = \Delta T_2 / \Delta T_1$, the amplification is quantified as $A = 2.0$, i.e., high-latitudes warms twice larger than low-latitudes. The meridional temperature

Table 1

Experiments by the EBM for various parameter settings from Experiments E1 to E4. The units are K for temperatures and PW for F and ε . The ice fraction a is dimensionless, and the corresponding ice–edge latitude (degree) is denoted by $a(\text{lat})$.

Exp.	F	a	ε	$a(\text{lat})$	T_1	T_2	T_G	$T_1 - T_2$	Note
E1	0	0	0	–	317	257	287	60	Rad. Equiv.
E2	5.5	0	0	–	298	277	287	20	Heat Trans.
E3	5.8	0.12	0	61	296	272	284	24	Cryosphere
E4	5.8	0.08	0.51	66	298	276	287	22	$2 \times \text{CO}_2$
E4–E3	0	–0.04	0.51	5	2	4	3	–2	$A = 2.0$

difference $T_1 - T_2$ is reduced by 2 K associated with the Arctic amplification, and the ice–edge retreats by 5° with the ice fraction change from 0.12 to 0.08. Note that the meridional heat flux F is tuned not to change by the global warming as seen in many climate models, since the decreased sensible heat flux offsets with the increased latent heat flux in the model.

[Fig. 2](#) plots the time change of the Arctic amplification A as a function of time (year) for the doubling CO_2 in E4. The model integration starts from the present climate state with a given radiative forcing ε . The result for E4 (black line) shows an increase of A that approaches to the equilibrium of $A = 2.0$. The e-folding time of the relaxation is approximately 5 years for the given heat capacity H . The same time integration is repeated by cutting the variation in ice–albedo feedback (red line) or by cutting the variation in meridional heat flux (blue). It is interesting to note that the Arctic amplification is reduced from 2.0 to 1.5 when the cryosphere is fixed at the present state. The doubling CO_2 induces the Arctic amplification without the ice–albedo feedback, but the result indicates that the ice–albedo feedback enhances the Arctic amplification. In contrast, the Arctic amplification indicates almost the same value when the meridional heat flux is fixed at the present state. The result indicates that the ice–albedo feedback is essential for the Arctic amplification.

4. Theoretical consideration for the equilibrium

Because the governing equation is simple, we can evaluate the temperature change for the equilibrium state by the variational method. According to the theoretical analysis for the steady state of the simple EBM, local temperature changes ΔT_1 and ΔT_2 can be explained by the variation in radiative forcing ($\Delta \varepsilon$), meridional heat flux (ΔF), and ice fraction (Δa), respectively.

$$\Delta T_1 = \frac{\Delta \varepsilon - \Delta F}{B} \quad (4)$$

$$\Delta T_2 = \frac{\Delta \varepsilon + \Delta F}{B} - 2\alpha S_2 \frac{\Delta a}{B} \quad (5)$$

Assuming that the variation in meridional heat flux is negligible as seen for E4–E3 in [Table 1](#), we can express the Arctic amplification $A = \Delta T_2 / \Delta T_1$ as below.

$$\frac{\Delta T_2}{\Delta T_1} = 1 - 2\alpha S_2 \frac{\Delta a}{\Delta \varepsilon} \quad (6)$$

Namely, the Arctic amplification occurs by the ice–albedo feedback in the right hand side of the equation, i.e., ice–fraction Δa decreases in response to the radiative forcing $\Delta \varepsilon$ by doubling CO_2 .

By adding the local temperature changes, we can derive the (global) mean temperature change (ΔT_G).

$$\frac{\Delta T_1 + \Delta T_2}{2} = \frac{\Delta \varepsilon}{2B} \left(1 + \frac{\Delta T_2}{\Delta T_1} \right) \quad (7)$$

It is interesting to note that the global warming may be amplified by the Arctic amplification. According to the model experiments E4–E3 in [Table 1](#), it is found that $A = 2.0$ causing $\Delta T_G = 3$ K. The result of the experiments may be compared with the equation above, by substituting $A = 2.0$ in the right hand side and $\Delta T_G = 3$ K in the left hand side. In case of no Arctic amplification, $A = 1.0$ and the global warming results in 2 K as predicted by the Planck response. Therefore, Arctic amplification enhances the global warming from 2 K to 3 K by the ice–albedo feedback in the model. Moreover, we can show that the total cooling by the long-wave radiation becomes a function of the Arctic amplification such as

Arctic Amplification Index (annual mean) Two Box Energy Balance Model

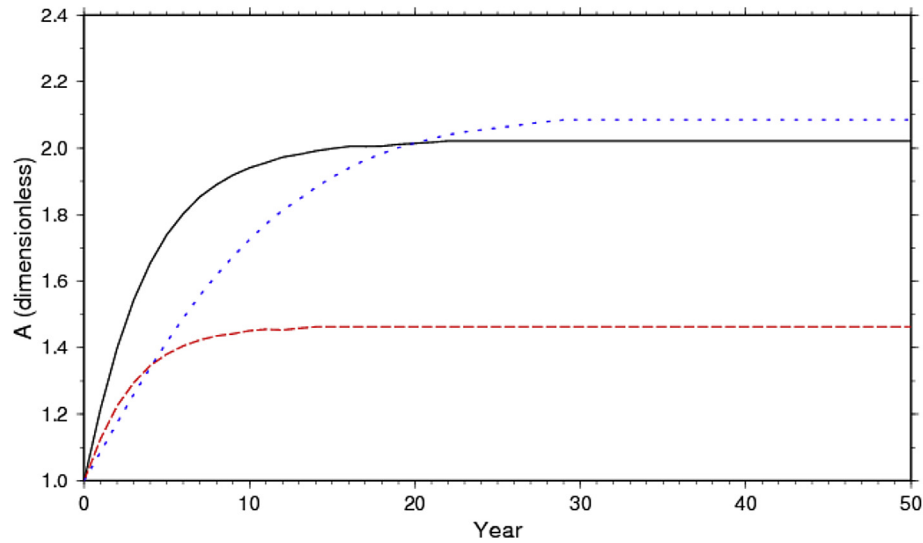


Fig. 2. Time change of the intensity of the Arctic amplification A for the doubling CO_2 experiment (black). The same experiments with a fixed ice fraction (red) or a fixed meridional heat flux (blue) starting from the present climate state are also plotted. (For interpretation of the references to colour in this figure legend, the reader is referred to the web version of this article.)

$(1+A)\Delta\epsilon = 1.54$ PW in response to the anthropogenic heating of $2\Delta\epsilon = 1.02$ PW. Therefore, the Arctic amplification appears to be an efficient cooling mechanism of the warmed climate system.

5. Consideration of internal variability

By the theoretical analysis of the simple EBM, we find that the variation of ice-albedo feedback causes the Arctic amplification, which enhances the global warming. Based on this fact, a hypothetical experiment is conducted by introducing a multi-decadal

variability of the ice-albedo feedback in reference to the observed long-term variation of the global mean temperature.

Fig. 3 plots the time variation of mean temperature (T_G) with the multi-decadal variability superimposed on a linear trend of the radiative forcing starting from 1900. There are two experiments with (red) and without (blue) the linear trend, given by 2.0 W m^{-2} per 100 years in the source sink term, mimicking the global warming. The multi-decadal variability is imposed by changing the ice fraction by ± 0.01 with positive peaks at 1910 and 1970, and negative peaks at 1940 and 2000 (see Akasofu, 2010; Ohashi and

N. H. Mean Temperature with Linear Trend Two Box Energy Balance Model

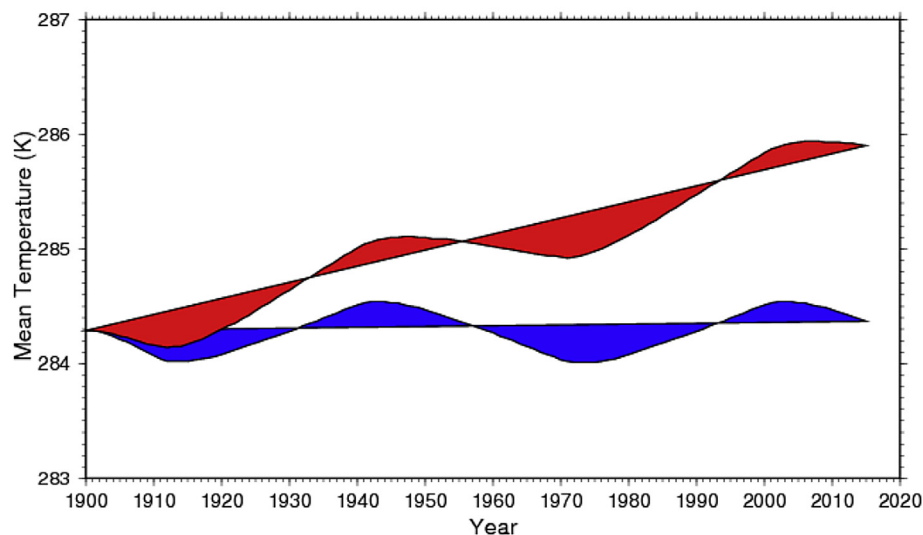


Fig. 3. Multi-decadal fluctuation of mean temperature forced by fluctuating ice fraction (-0.01 and $+0.01$ per 30 years). Blue: experiment with no CO_2 change, red: experiment with linear trend of CO_2 (2.0 W/m^2 per 100 years). (For interpretation of the references to colour in this figure legend, the reader is referred to the web version of this article.)

Correlation map for Albedo and Albedo Northern hemisphere (0 N – 90N, 0E – 360E) 1958/59 – 2011/12 DJF

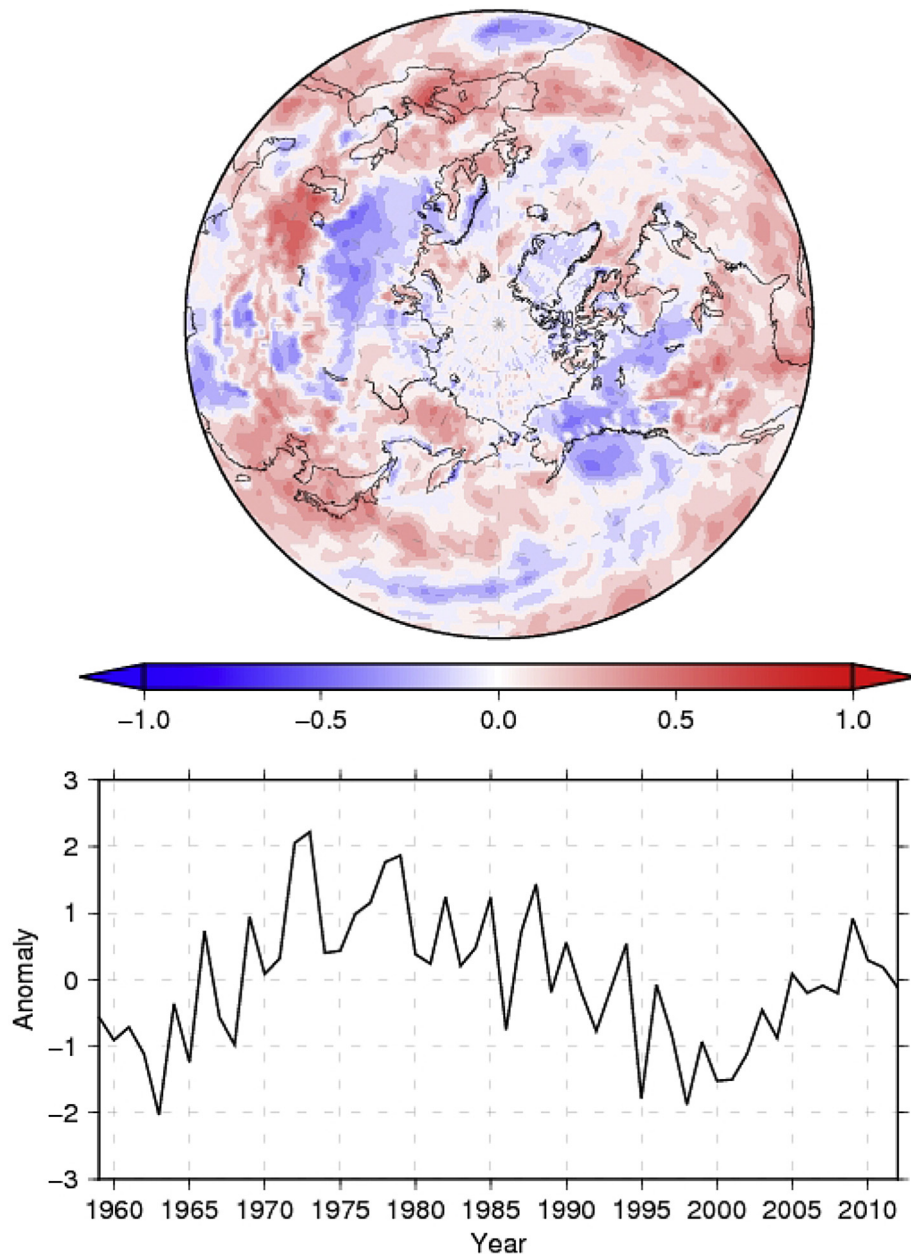


Fig. 4. Time series of mean planetary albedo in the Northern Hemisphere, and its correlation map with planetary albedo itself.

Tanaka, 2010). As expected, the internal variability in ice-albedo feedback by 10% largely influences the mean temperature showing warm 1940s, cold 1970s, and warm 2000s. This is a hypothetical multi-decadal variability, mimicking the internal variability of the Atlantic multi-decadal oscillation (AMO) or Pacific decadal oscillation (PDO), or Arctic oscillation (AO). The observational evidence of such an oscillation will be discussed in the next section. There is a time lag about 5 years in the mean temperature in response to the change in ice fraction.

It is important to mention that the linear trend after the year 2000 cancels out with the negative trend of the internal variability,

indicating the warming hiatus for this period. Moreover, the rapid global warming for 1970–2000 is caused by the superposition of the internal variability and the linear trend in the model. Although the results are based on the hypothesis, multi-decadal variability in ice-albedo feedback is the subject of the next section.

6. Time change of planetary albedo

The multi-decadal variability of mean temperature is reproduced by the change in ice-albedo feedback in our model. Not only the ice fraction, but also the short wave radiation and albedo may

Correlation map for SAT and Albedo
Northern hemisphere (0 N – 90N, 0E – 360E)
1958/59 – 2011/12 DJF

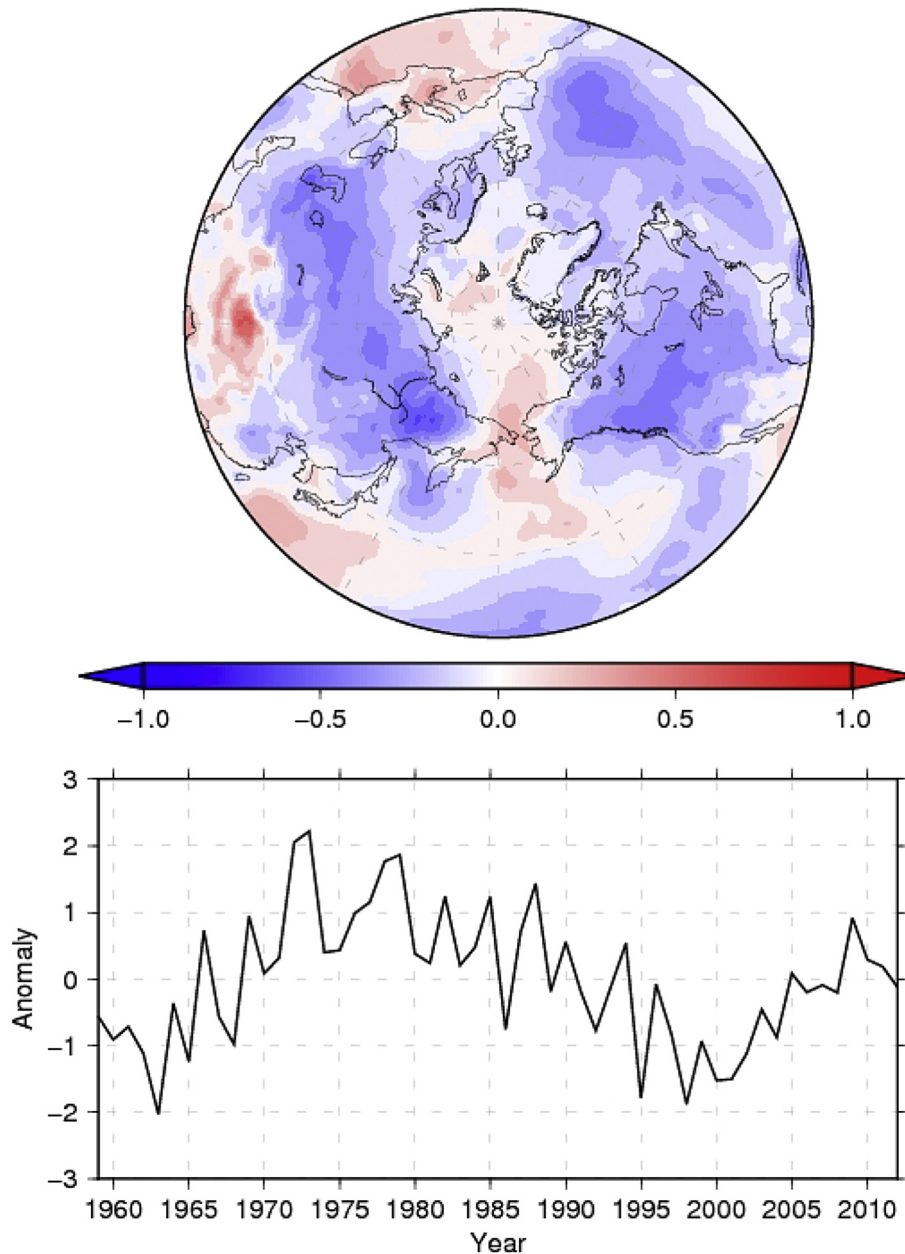


Fig. 5. Time series of mean planetary albedo in the Northern Hemisphere, and its correlation map with surface air temperature.

be important to control the ice-albedo feedback. Although the ice fraction is the state variable in the model, the planetary albedo is the key variable in the energy balance model in Fig. 1. For this reason, we conducted data analysis for the planetary albedo using the long-term reanalysis data.

Fig. 4 illustrates the time variation of the mean planetary albedo in winter (DJF) averaged in the Northern Hemisphere evaluated from JRA-55 reanalysis data (Japan 55-year Reanalysis; JMA: Japan Meteorological Agency). The monthly mean time series data are used to obtain the correlation map for the planetary albedo itself in the Northern Hemisphere. The analysis result shows interesting

multi-decadal variation with positive peak anomaly at 1970 and negative peak anomaly at 2000. The planetary albedo started to increase after 2000 when the warming hiatus occurred. The time change of the mean planetary albedo in Fig. 4 partly supports the internal variability demonstrated in Fig. 3, at least for the recent 55 years. The time series data are normalized. The mean values are ranging from 0.319 to 0.326. Multiplied by the strong solar radiation, the 1% variation of planetary albedo is large enough to modify the linear warming trend. The self-correlation map shows positive values in most of the area, especially over the Europe, Far East, and USA. However, negative areas are seen over northwestern Siberia

Correlation map for Snow and Albedo
Northern hemisphere (0 N – 90N, 0E – 360E)
1979/80 – 2011/12 DJF

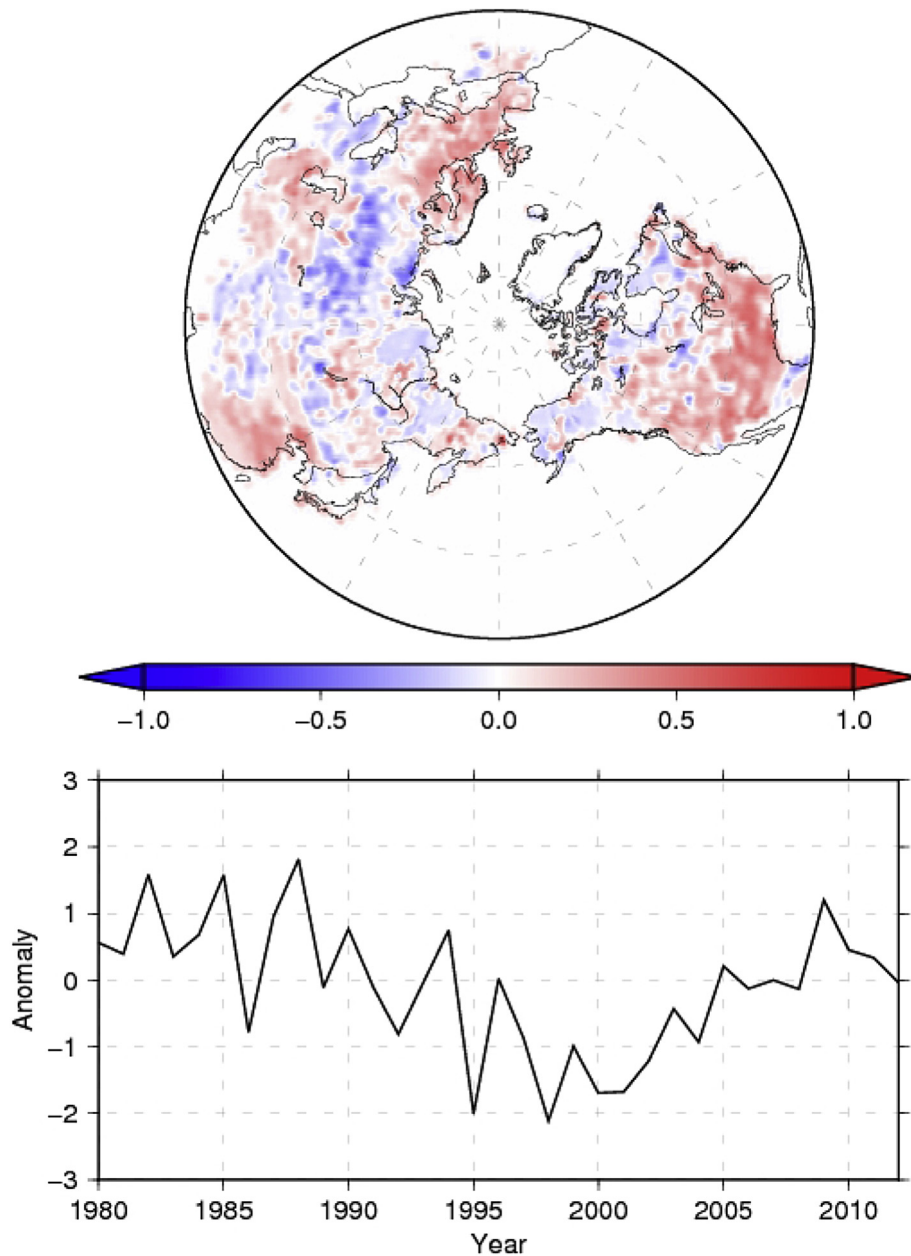


Fig. 6. Time series of mean planetary albedo in the Northern Hemisphere, and its correlation map with snow depth on the land.

and Alaska. The poor correlation at this area is linked to the AO as will be discussed later.

Fig. 5 illustrates the correlation map for surface air temperature (SAT) with the time series of the mean planetary albedo. The correlation map shows negative values over Siberia, North America, and North Atlantic Ocean, and positive values over the Arctic Ocean. The temperature response is consistent with albedo change at the subarctic where the solar radiation reaches in DJF.

Fig. 6 illustrates the correlation map for snow depth in DJF with the time series of the mean planetary albedo. Note that the period is

shorter than SAT because the ERA-interim data are used for the snow depth data. Positive areas are seen over North America, Europe, and Far East, and negative areas over western Siberia. It is found that the snow depth shows good correlation with planetary albedo in most areas except for western Siberia. The area of poor correlation implies the importance of cloud radiative process for the albedo change.

It should be noted that the time series of the mean planetary albedo in Figs. 4–6 are compared for ERA-interim data and JRA-55 data, and the same long-term variations are confirmed with a

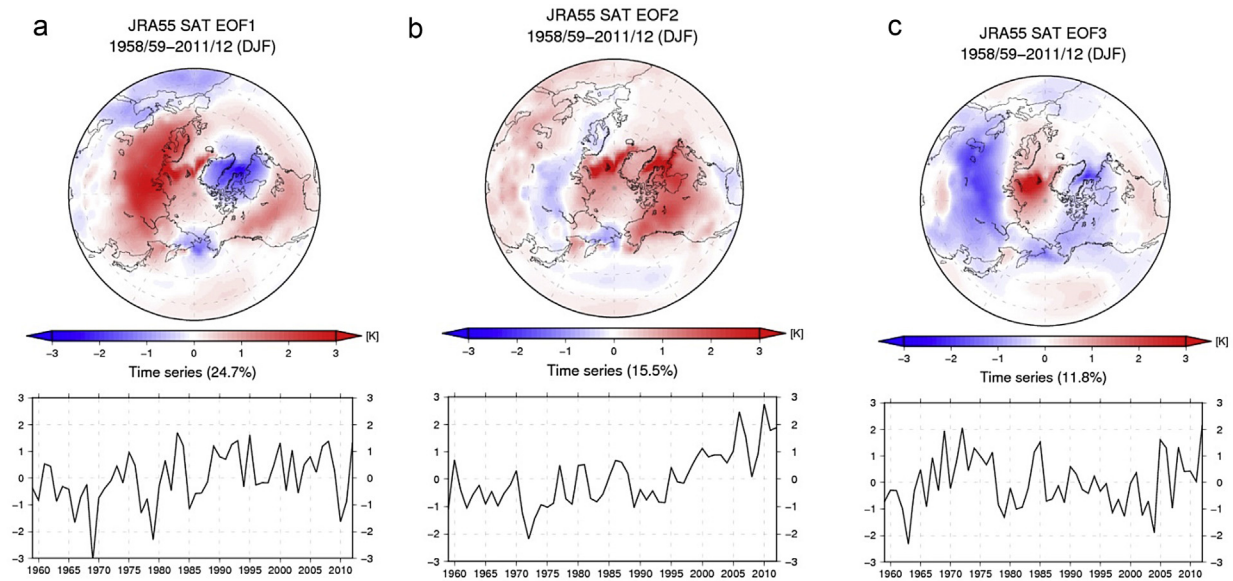


Fig. 7. (a) Arctic oscillation mode obtained by EOF-1 of surface air temperature (SAT) and its time series. (b) Arctic amplification mode obtained by EOF-2 of surface air temperature (SAT) and its time series. (c) Barents Sea mode obtained by EOF-3 of surface air temperature (SAT) and its time series.

quantitative agreement.

7. Connection to the Arctic oscillation

Finally, the connection between the Arctic oscillation and planetary albedo is investigated in this section. Fig. 7a illustrates the structure and the time series of the Arctic oscillation mode evaluated as the EOF-1 (24.7% variance) of the surface air temperature (SAT) using the JRA-55 data for DJF from 1958/59 to 2011/12. The AO index evaluated by SAT is a little different from that obtained by sea level pressure (SLP) as presented by Nagato and Tanaka (2012), but the long-term variability seems consistent with each other. The spatial pattern of temperature shows positive values over Siberia and North America and negative values over Greenland for AO positive. This spatial pattern was almost identical to the global warming pattern during 1970–1990. It was said once in 1990s that 40% variance of the global warming can be explained by the natural variability of Arctic oscillation (Shindell et al., 1999). The time series shows decreasing trend before 1970, increasing trend from 1970 to 1990, and decreasing trend from 1990 to 2010. The global mean temperature keeps increasing after 1990, but the AO index started to decrease from the positive in 1990s to negative in 2000s. For this reason, AO was once excluded from the possible cause of the global warming. However, the increasing temperature trend appears to halt after 2000 indicating major discrepancy from the climate model predictions, known as warming hiatus. Warm Arctic and cold mid-latitudes is the main characteristic during the warming hiatus, showing an agreement with AO negative pattern during 2000s. Although the details are different, the multi-decadal variation is similar to that for the planetary albedo in Fig. 4 with opposite sign.

Fig. 7b illustrates the distribution and time series of SAT for the EOF-2 (15.5% variance). Notable warming trend occurs in the Arctic and North America. In Nagato and Tanaka (2012), this pattern was considered as the Arctic amplification pattern induced by the anthropogenic radiative forcing due to the increasing greenhouse gases, using the NCEP/NCAR reanalysis data. The same results are confirmed in this study using the JRA-55 reanalysis data.

Fig. 7c illustrates the distribution and time series of SAT for the

EOF-3 (11.8% variance). The distribution indicates positive values around Barents Sea surrounded by negative values in the sub-arctic and mid-latitudes especially at Siberia and North America. From this pattern, this mode is referred to as Barents Sea mode in this study. The time series shows an interesting multi-decadal variation with a positive peak at 1970, negative peak at 2000 and increasing trend during the warming hiatus period after 2000, which is similar to the mean planetary albedo in Fig. 4. The time variation seems to link to the multi-decadal variation of the AMO (see Levitus et al., 2009). The regression analysis shows that the Northern Hemisphere mean temperature of the EOF-3 is -0.16 K, which can explain the long-term variation of the mean temperature in Fig. 3 superimposed on the linear trend by the anthropogenic radiative forcing. It is shown by Nagato and Tanaka (2012) that the Northern-Hemisphere mean surface temperature associated with the AO is close to zero, although it has the largest regional variance. In this regards, the AO mode is important for the local variation in temperature, and Barents Sea mode seem to link to the multi-decadal variability of the mean temperature. Both modes show the characteristics of warm Arctic and cold mid-latitudes, although the center is located at Greenland for AO and at Barents Sea for the Barents Sea mode (refer to Mori et al., 2014).

Fig. 8 illustrates the correlation map for planetary albedo with the time series of the AO index evaluated as the EOF-1 of the SAT as in Fig. 7a. There are positive values over Siberia and North Atlantic, Greenland, and negative values at Europe and the Far East in mid-latitudes surrounding the positive values in high-latitudes. The correlation changes the sign between the northern and southern Siberia. The anomaly pattern of albedo describes that when AO index is positive, the albedo is high at high-latitudes and is low at mid-latitudes. Conversely, when AO index is negative, the albedo is low at high-latitudes and is high at mid-latitudes. The pattern is consistent with warm Arctic and cold mid-latitudes during the negative AO index as seen for the warming hiatus period. The result suggests that the negative values over northwestern Siberia in Fig. 4 reflects the influence of the AO.

Fig. 9 illustrates the correlation map for SAT with the time series of planetary albedo averaged over the northwestern Siberia ($55\text{--}67^\circ$ N, 30 to 120° E) as seen in Fig. 8. The time series shows

Correlation map for Albedo and SAT EOF1
Northern hemisphere (0 N – 90N, 0E – 360E)
1958/59 – 2011/12 DJF

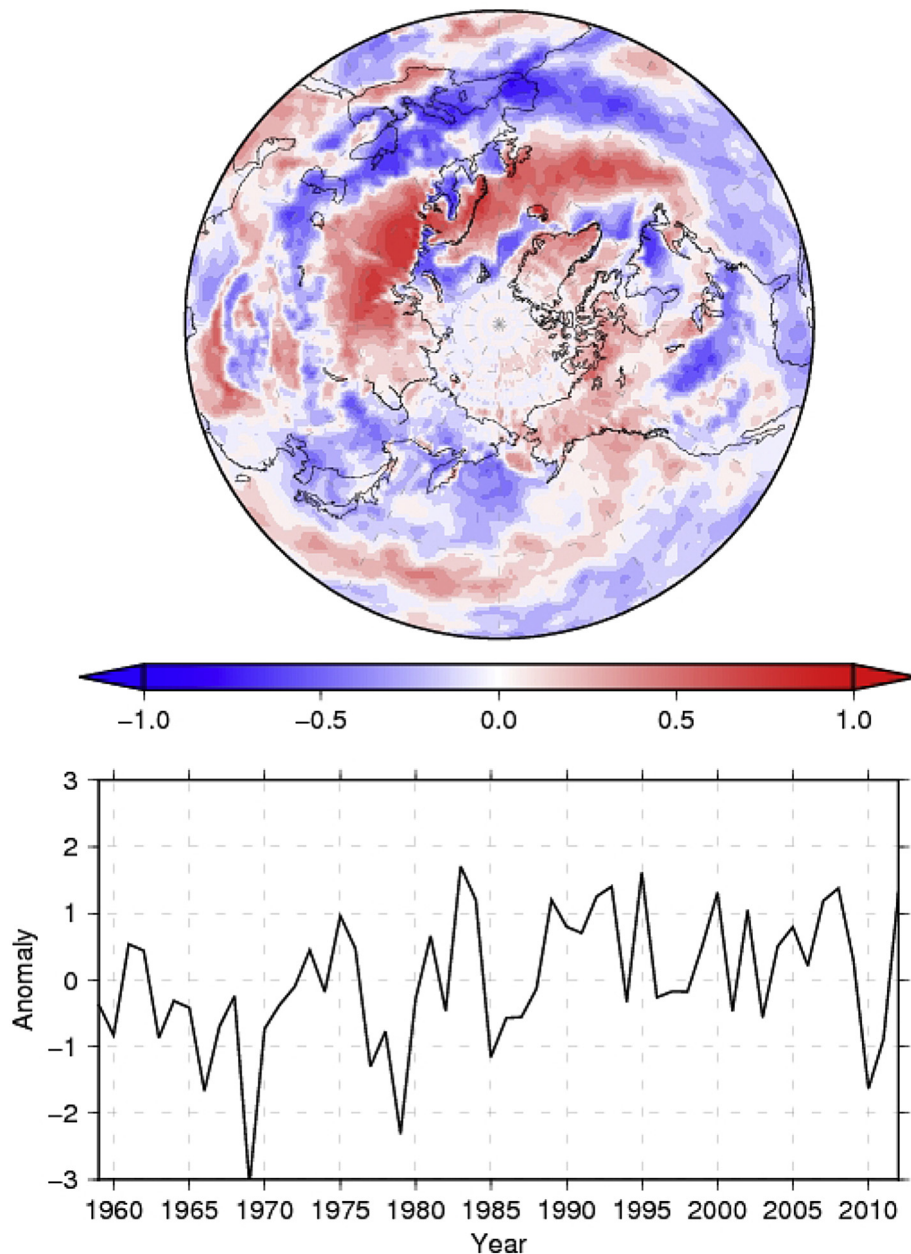


Fig. 8. Time series of the AO index in Fig. 7a, and its correlation map with planetary albedo.

decreasing trend before 1970, increasing trend from 1970 to 1990, and decreasing trend from 1990 to 2010. The correlation map with this time series shows negative values over Greenland and Alaska which is surrounded by the positive values over Siberia and North America. The pattern is very similar to the Arctic oscillation in Fig. 7a. North Siberia seems to be a key region for AO, indicating a significant positive correlation between the AO index and the planetary albedo change there. Conversely, the AO index indicates a significant negative correlation with the planetary albedo averaged over the mid-latitudes as seen in Fig. 8.

8. Summary and discussion

The global warming hiatus is an important observational fact to be explained clearly for the global warming projection study (see Trenberth and Fasullo, 2013). Responding to the monotonic increase in CO₂, many of the climate models predict a monotonic warming in the model ensemble mean, with natural and internal variability superimposed on it. The natural and internal variability has been considered to be sufficiently small compared to the warming speed by the anthropogenic increase of CO₂. However, the warming hiatus is explained by the natural and internal variability of the climate system superimposed on the monotonic trend. This

Correlation map for SAT and Albedo
North Eurasia (55 N – 67N, 30E – 120E)
1958/59 – 2011/12 DJF

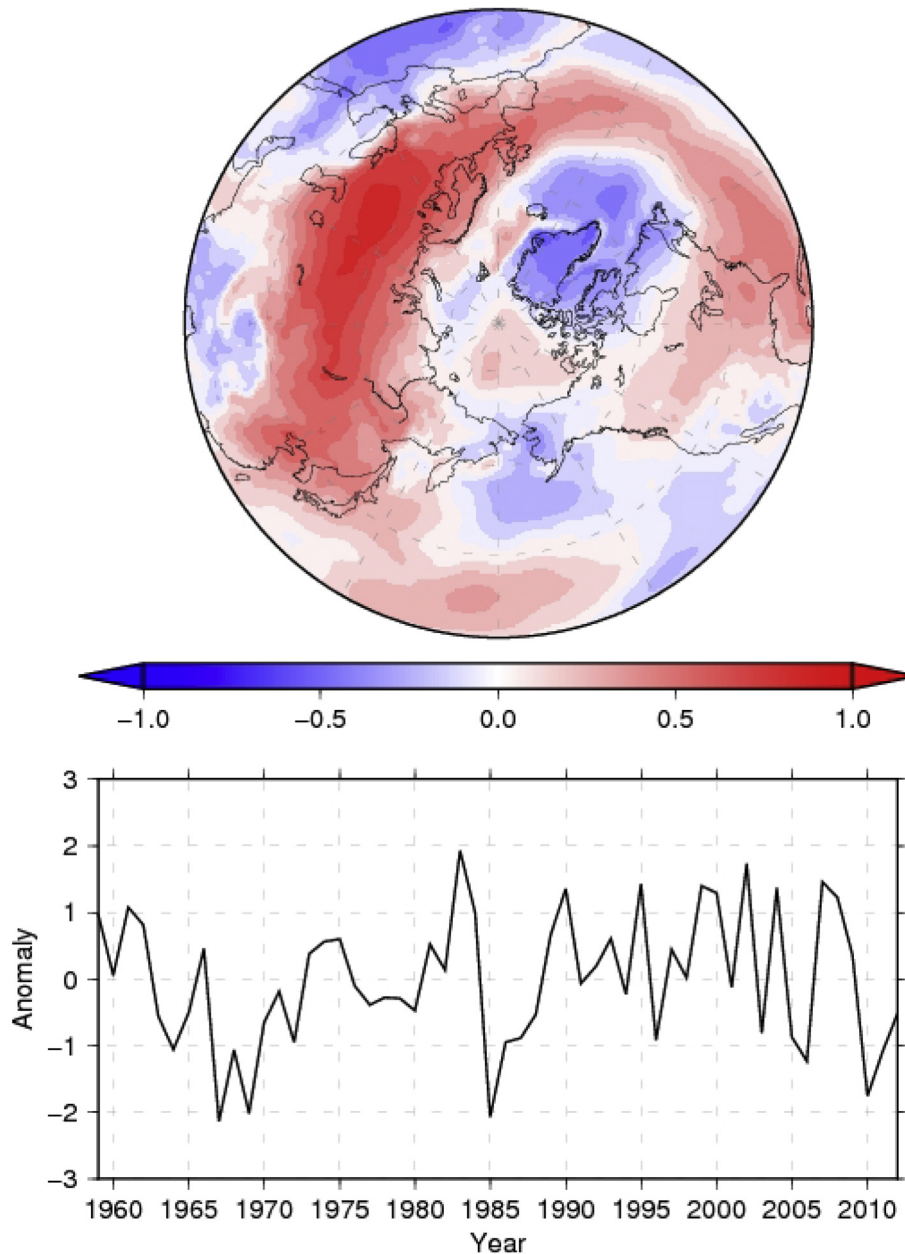


Fig. 9. Time series of mean planetary albedo over northwestern Siberia (55–67° N, 30–120° E) and its correlation map with surface air temperature.

fact supports that the natural and internal variability in multi-decadal time scale has a comparable magnitude as the anthropogenic global warming trend.

In this study, a simple energy balance model (EBM) was integrate in time, considering a hypothetical long-term variability in ice-albedo feedback mimicking the observed multi-decadal temperature variability. The natural variability was superimposed on the linear warming trend due to the increasing anthropogenic radiative forcing of CO₂. The result demonstrates that the superposition of the natural variability and the background linear trend can offset with each other to show the warming hiatus for some

period. It is also stressed that the rapid warming during 1970–2000 can be explained by the superposition of the natural variability and the background linear trend at least within the simple model.

The key process of the changing planetary albedo in multi-decadal time series is investigated using the JRA-55 reanalysis data and ERA-interium data. It is found that the planetary albedo increased for 1958–1970, decreased for 1970–2000, and increased for 2000–2012, as expected by the simple EBM experiments. The multi-decadal variability in the planetary albedo is compared with the time series of the AO mode and Barents Sea mode of surface air temperature. It is shown that the recent AO negative pattern of

EOF-1 with the warm Arctic and cold mid-latitudes is in good agreement with planetary albedo change indicating negative anomaly in high-latitudes and positive anomaly in mid-latitudes. Moreover, the Barents Sea mode of EOF-3 with the warm Barents Sea and cold mid-latitudes shows multi-decadal variability similar to the time series of mean planetary albedo. The result suggests that the Barents Sea mode, which is presumably activated by the AMO, results in high albedo in mid-latitudes due to the increased snow fall as well as the changing cloud radiative process during the warming hiatus period (see Mori et al., 2014). Although further studies are needed, the natural variabilities of both the AO mode and Barents Sea mode indicate some possible link to the planetary albedo as suggested by the simple EBM to cause the warming hiatus in recent years.

Acknowledgements

We would like to thank Dr. V. A. Alexeev of University of Alaska for their constructive comments. We appreciate the help by Ms. T. Umino, former graduate student of the University of Tsukuba. This study was partly supported by the GRENE Arctic Climate Research Project.

References

- Akasofu, S.I., 2010. On the recovery from the little ice age. *Sci. Res. Open Access* 2 (11), 1211–1224. <http://file.scirp.org/Html/3217.html>.
- Alexeev, V.A., Jackson, C.H., 2012. Polar amplification: is atmospheric heat transport important? *Clim. Dyn.* <http://dx.doi.org/10.1007/s00382-012-1601-z>.
- Graversen, R.G., Wang, M., 2009. Polar amplification in a coupled climate model with locked albedo. *Clim. Dyn.* 33, 629–643.
- Hirata, Y., Shimo, Y., Tanaka, H.L., Aihara, K., 2011. Chaotic properties of the Arctic oscillation index. *SOLA* 7, 33–36.
- Kay, J.E., Holland, M.M., Bitz, C., Blanchard-Wrigglesworth, E., Gettelman, A., Conley, A., Bailey, D., 2012. The influence of local feedback and northward heat transport on the equilibrium Arctic climate response to increased greenhouse gas forcing in coupled climate models. *J. Clim.* 25, 5433–5450.
- Kosaka, Y., Xie, S.-P., 2013. Recent global-warming hiatus tied to equatorial Pacific surface cooling. *Nature* 501, 403–407.
- Langen, P.L., Alexeev, V.A., 2007. Polar amplification as a preferred response in an idealized aqua planet GCM. *Clim. Dyn.* 29, 305–317.
- Levitus, S., Matishov, G., Seidov, D., Smolyar, I., 2009. Barents Sea multidecadal variability. *Geophys. Res. Lett.* 36, L19604. <http://dx.doi.org/10.1029/2009GL039847>.
- Manabe, S., Stouffer, R.J., 1980. Sensitivity of a global climate model to an increase of CO₂ concentration in the atmosphere. *J. Geophys. Res.* 85, 5529–5554.
- Manabe, S., Wetherald, R.T., 1975. The effect doubling the CO₂ concentration on the climate of a general circulation model. *J. Atmos. Sci.* 32, 3–15.
- Mori, M., Watanabe, M., Shiogama, H., Inoue, J., Kimoto, M., 2014. Robust Arctic sea-ice influence on the frequent Eurasian cold winters in past decades. *Nat. Geosci.* <http://dx.doi.org/10.1038/ngeo2277>.
- Nagato, Y., Tanaka, H.L., 2012. Global warming trend without the contributions from decadal variability of the Arctic oscillation. *Polar Sci.* 6, 15–22.
- Ohashi, M., Tanaka, H.L., 2010. Data analysis of recent warming pattern in the Arctic. *SOLA* 6A, 1–4.
- Overland, J.E., Wood, K.R., Wang, M., 2011. Warm Arctic - cold continents: climate impacts of the newly open Arctic Sea. *Polar Res.* 30, 15787. <http://dx.doi.org/10.3402/polar.v30i0.15787>.
- Shindell, D.T., Miller, R.L., Schmidt, G.A., Pandolfo, L., 1999. FSimulation of recent northern winter climate trends by greenhouse-gas forcing. *Nature* 399, 452–455.
- Thompson, D.W.J., Wallace, J.M., 1998. The Arctic oscillation signature in the wintertime geopotential height and temperature fields. *Geophys. Res. Lett.* 25, 1297–1300.
- Trenberth, K.E., Fasullo, J.T., 2013. An apparent hiatus in global warming? *Earth's Future* 1, 19D–32D.
- Umino, T., 2014. A Theoretical Study of Arctic Amplification and Arctic Oscillation Using an Energy Balance Model. Master Thesis, Life and Environmental Science, University of Tsukuba, p. 40 (in Japanese).
- Wallace, J.M., Thompson, D.W.J., 2002. Annular modes and climate prediction. *Phys. Today* 55, 28–33.
- Watanabe, M., Shiogama, H., Tatebe, H., Hayashi, M., Ishii, M., Kimoto, M., 2014. Contribution of natural decadal variability to global warming acceleration and hiatus. *Nat. Clim. Change* 4, 893–897.
- Yoshimori, M., Yokohata, T., Abe-Ouchi, A., 2009. A comparison of climate feedback strength between CO₂ doubling and LGM experiments. *J. Clim.* 22, 3374–3395.
- Yoshimori, M., Abe-Ouchi, A., Watanabe, M., Oka, A., Ogura, T., 2014. Robust seasonality of Arctic warming processes in two different versions of MIROC GCM. *J. Clim.* 27, 6358–6375.